



Examining the Compressive Behavior of SFRC and SCC Using Finite Element and Experimental Methods

Muna M. A. Hano ¹, Salwa M. A. Hano ¹, Hesham S. Al-Rawe ^{2*}

¹ Department of Civil Engineering, College of Engineering, University of Mosul, Mosul, 41001, Iraq.

² Department of Building and Construction, Engineering Technical College of Mosul, Northern Technical University, Mosul, Iraq.

Received 18 December 2024; Revised 19 February 2025; Accepted 27 February 2025; Published 01 March 2025

Abstract

The compressive behavior of various kinds of concrete, including plain concrete, steel fiber-reinforced concrete (SFRC), and self-compacting concrete (SCC), was investigated experimentally in this paper and simulated using finite element analysis through ABAQUS software. Thirty specimens were cast and tested with two concrete compressive strengths (20 and 30 MPa). Steel fibers were added at volume fractions of (0, 0.4, and 0.75)%, while SIKAVISCOCRETE-5930 IQ was incorporated at (0.8 and 1.8)% by weight of cement. The results showed that the compressive strength of the tested specimens increased with the increase of fibers and SIKAVISCOCRETE-5930 IQ dosages. The FEA results exhibited a good agreement with those from the experimental work in terms of the stress-strain relationships for plain, SFRC, and SCC. A Student's t-test was performed on both experimental and FE analysis outcomes, and the difference among them was found to be statistically insignificant. The accuracy of numerical modeling in predicting concrete behavior under compression is supported by the findings of this study, and the effectiveness of steel fibers and SIKAVISCOCRETE-5930 IQ in developing the compressive strength of concrete is also highlighted.

Keywords: Concrete; Finite Element Analysis; Compressive Behavior; Steel Fiber; Superplasticizer (SIKAVISCOCRETE-5930 IQ).

1. Introduction

Concrete is one of the major construction materials, consisting of cement, fine and coarse aggregates mixed with water. It is widely used due to the availability of its raw materials, high workability, and durability [1-3]. However, concrete has some limitations regarding its poor chemical resistance, ductility, and tensile strength [4, 5]. Therefore, researchers have studied and discussed various modifications to enhance its performance through the incorporation of fibers with different chemical admixtures. Fiber-reinforced concrete, among numerous construction materials, is considered the most promising and cost-effective option. Using small, closely spaced, and uniformly distributed fibers in concrete helps to transform its brittle nature into a more stable and strong one [6-8]. Ayub et al. [9] investigated the use of fiber-reinforced concrete beams and found that adding fibers enhances their ductility and carrying capacity. Rashidi et al. [10] examined the impact of utilizing steel fibers on the mechanical properties of concrete. They concluded that applying the optimal fiber content improves both the compressive and tensile strength of concrete.

Self-compacting concrete (SCC) is one of the available solutions to develop characteristics of concrete. SCC is an advanced technique presented in the 1980s. It helps in providing concrete mixtures that can flow and fill the formworks under gravity only without any need for mechanical actions. Using SCC decreases the required costs of concrete construction due to its special durability, performance in surface finishing, and reliability of structures. Al-Jubory et al. [11] conducted a review about mix designs of SCC. They concluded that there are no clear or specific

* Corresponding author: hesham.salim@ntu.edu.iq

 <http://dx.doi.org/10.28991/CEJ-2025-011-03-017>



steps for the design of SCC, indicating the requirement for additional research. Akinpelu et al. [12] demonstrated the structural performance of deep beams produced with SCC. The outcomes from FEM matched well with the experimental ones, as they both showed better structural reliability.

The finite element method (FEM) is a theoretical analysis for reinforced concrete (RC) structures. Several recent studies have approved the capability of FEM in accurate modeling for the behavior of fiber-reinforced and self-compacting concrete elements. Chowdhury et al. [13] conducted experimental and numerical studies on SFRC and found that the tested specimens showed an increase in their compressive strength up to 17% and splitting tensile strength up to 146% in comparison to the reference ones. Saffar & Aghwan [14] developed a model using FEM to analyze the I-section of concrete beams reinforced with fibers that are gathered from previous studies. The findings were compared and explored a good agreement in terms of crack patterns, ultimate failure loads, and load-deflection curves.

This study establishes an FE model considering the compressive response of self-compacting concrete (SCC) and steel fiber-reinforced concrete (SFRC). The model was developed using ABAQUS software and was validated using experimentally tested specimens. Stress-strain behavior is focused on discussing how concrete performance can be affected by steel fibers and self-compacting properties. SFRC and SCC have previously been studied separately; however, the current research provides comprehensive FE models of both materials that could accurately predict the compressive behavior of the specimens. This paper represents an effort to cover this gap in which the adopted model can serve as a design tool in future structural analyses and designs.

2. Concrete Materials and Mix Details

- **Ordinary Portland cement (OPC):** Both physical and chemical characteristics of OPC used in this research, meeting the requirements of IQS [15], are listed in Tables 1 and 2, respectively.

Table 1. Physical characteristics of OPC

Properties	Unit	Value	Specifications (IQS:5/2019) [15]
Standard Consistency (W/C)	-	0.28	-
Initial Setting Time	M	105	≥ 45
Final Setting Time	M	195	≤ 600
Compressive Strength (3 days)	MPa	20.1	≥ 10
Compressive Strength (28 days)	MPa	43.5	≥ 32.5

Table 2. Chemical characteristics of OPC

Chemical Components	Value (%)	Specifications (IQS:5/2019) [15]	Chemical Components	Value (%)
SiO ₂	20.20	-	C ₃ S	54.12
AL ₂ O ₃	4.99	-	C ₂ S	17.09
Fe ₂ O ₃	3.97	-	C ₃ A	6.49
CaO	63.85	-	C ₄ AF	12.09
MgO	2.77	≤ 5	L.S.F	95.88
SO ₃	2.01	≤ 2.5	Solid solution	17.23
Free lime	1.82	-	-	-
Loss on ignition	0.14	≤ 4	-	-
Insoluble residue	1.30	≤ 1.5	-	-
Total	101.04			

- **Coarse and fine aggregates:** Coarse aggregate is available locally, passing through sieve No. 19 mm and having a specific gravity of 2.7 with 0.68% of absorption. The sieve analysis was conducted based on Iraqi specifications IQS [16] as shown in Table 3. Fine aggregate is available locally with a sieve analysis conducted according to the Iraqi specifications IQS [16], as shown in Table 4.

Table 3. Sieve Analysis of Coarse Aggregate

Sieves No.	Passing (%)	IQS specifications [16]
¾"	100	100
½"	93	100-90
3/8"	57.4	85-50
4	6.4	0-10

Table 4. Sieve Analysis of Fine Aggregate

Sieves No.	Passing (%)	IQS specifications [16]
4.75 (No.4)	100	100-90
2.36 (No.8)	87.32	100-75
1.18 (No.16)	70.94	90-55
0.6 (No.30)	56.26	59-35
0.3 (No.50)	28.61	30-8
0.15 (No.100)	3.91	10-0

- **Steel fibers:** Steel fibers are defined as elongated wire strands that are deformed and trimmed to the required length. They are used to enhance the strength of concrete, mortar, and other similar composite substances. Figure 1 illustrates the steel fibers used in this research, and their physical characteristics are listed in Table 5.



Figure 1. Steel fibers

Table 5. Technical data for the used steel fibers

Fiber length mm (in)	50 (2)
Equivalent diameter (mm)	1.0 ± 0.03
Tensile strength (MPa ±5%)	850
Thickness of fiber (mm)	0.5
Width (mm)	1.4

- **Superplasticizer (SP):** Superplasticizer type SIKA-VISCOCRETE -5930 IQ was used with two ratios of 0.8% and 1.8% to maintain the self-compacting concrete. It is also used in the original mix to maintain the workability and to achieve the required concrete compressive strength.
- **Compressive strength of concrete:** Two mixtures (20 and 30) MPa were prepared as demonstrated in Table 6. A series of trail mixes were conducted to achieve the desired strength.

Table 6. Details of concrete mixtures

	Mix (C:S:G)/W	Strength (MPa)	Slump (cm)	Cement (kg/m ³)	Sand (kg/m ³)	Gravel (kg/m ³)	Water (kg/m ³)	Fiber (kg/m ³)	SIKA-VISCOCRETE - 5930 IQ (gm)
Group 1	1:2.9:3.25/0.58	20	5	311	902	1011	180	0	0
	1:2.9:3.25/0.58	20	4	311	902	1011	180	30	0
	1:2.9:3.25/0.58	20	2.75	311	902	1011	180	60	0
Group 2	1:2.27:2.32/0.427	30	2	404	917	937	173	0	125
	1:2.27:2.32/0.427	30	20	404	917	937	173	30	185
	1:2.27:2.32/0.427	30	16	404	917	937	173	60	245
Group 3	1:2.9:3.25/0.58	20	5	311	902	1011	180	0	0
	1:2.9:3.25/0.58*	20	-	311	902	1011	180	0	46.2
	1:2.9:3.25/0.58*	20	-	311	902	1011	180	0	102.8
Group 4	1:2.27:2.32/0.427	30	2	404	917	937	173	0	125
	1:2.27:2.32/0.427*	30	-	404	917	937	173	0	240.68
	1:2.27:2.32/0.427*	30	-	404	917	937	173	0	370.3

* The slump was not measured for the self-compacting mixtures

3. Fabrication and Testing of Samples

A total of thirty cylinder specimens of (300*150) mm were cast and tested according to the ASTM C39/C39-20 [17]. The slump test was measured for each mixture in respect to the ASTM C143 guidelines [18]. The cylindrical specimens were poured and left for (24) hours to allow setting of concrete. Then, they had (28) days of curing in water in order to be ready for the testing process.

Specimens are classified into four groups as shown in Table 7. The first and second groups included nine specimens per each cast with concrete containing two ratios of steel fibers having volume fractions of (0, 0.4, and 0.75)% and with a concrete compressive strength of 20 MPa and 30 MPa, respectively. The third group included six specimens cast with concrete containing two ratios of SP (0.8 and 1.8) % and a compressive strength of 20 MPa. Their results were compared with the control specimens from the first group. The fourth group included six specimens cast with concrete containing SP of (0.8 and 1.8)% and compressive strength of 30 MPa. Their results were compared with the control specimens from the second group.

Table 7. Research methodology

Thirty-cylinder specimens			
Group 1	Group 2	Group 3	Group 4
Nine cylinders (average of each three is reported)	Nine cylinders (average of each three is reported)	Six cylinders (average of each two is reported)	Six cylinders (average of each two is reported)
Compressive strength is 20 MPa	Compressive strength is 30 MPa	Compressive strength is 20 MPa	Compressive strength is 30 MPa
Three ratios of steel fiber (0, 0.4 and 0.75)%	Three ratios of steel fiber (0, 0.4 and 0.75)%	Two ratios of super (0.8 and 1.8)	Two ratios of super (0.8 and 1.8)
Test the specimens for compressive stress-strain relation			
Create a general FE model to simulate the behavior of fiber-reinforced concrete			
Compare the results from the FE model with the experimental ones			

The specimens were tested using a compression testing machine as shown in Figure 2, and a steel gauge was installed to measure the response resulting from the application of incremental loads at a loading ratio of 0.3 MPa/sec.



Figure 2. Samples ready for testing

4. Results and Discussion

4.1. Stress-Strain Relationships

Figures 3-a and 3-b show the stress versus strain relationships for specimens in groups 1 and 3, which have 20 MPa of compressive strength. Group 1 has 0, 0.4, and 0.75% of steel fibers, while group 3 has 0, 0.8, and 1.8% of SP. Figures 4-a and 4-b show the stress versus strain relationships for groups 2 and 4 of specimens with a concrete compressive strength equal to 30 MPa. Group 2 has a steel fiber content of 0, 0.4, and 0.75%, while group 4 has an SP content of 0, 0.8, and 1.8%. Figures 3 and 4 exhibit similar behavior, showing an increase in stiffness and peak load with the increase of the steel fiber and SP ratios; this matched the results from the literature.

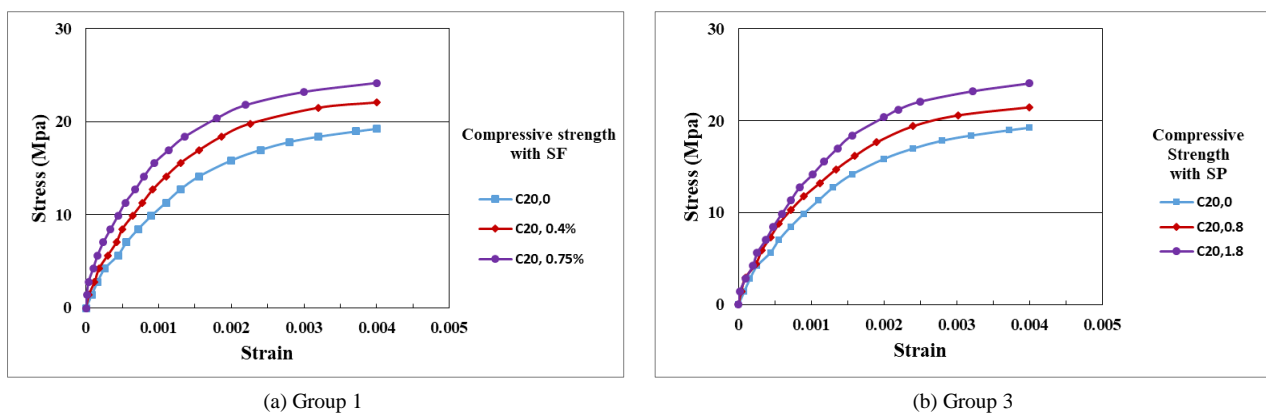


Figure 3. Stress-strain relationships for specimens in groups 1 and 3

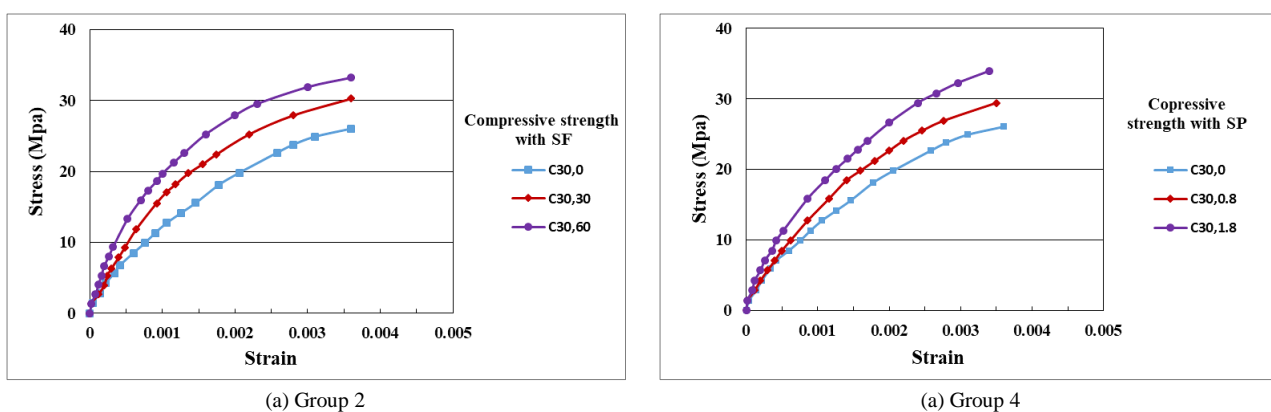


Figure 4. Stress versus strain for specimens in groups 2 and 4

At the peak, the specimens showed an increase in stress of approximately 15% and 26% in group 1, 11%, and 25% in group 2 for steel ratios of 0.4% and 0.75%, respectively. Also, at the peak, the specimens exhibited compressive stress increases of approximately 16% and 28% in group 3, and 13% and 30% in group 4 for SP ratios of 0.8 and 1.8%, respectively (as listed in Table 8). When the ratios of added steel fibers increased, the ductility and crack resistance of the concrete improved. This resulted in smoother and more gradual stress-strain post-peak behavior. In the same way, the enhanced workability of the SCC improved the particle distribution and therefore increased the compressive strength and the stress concentration.

Table 8. Percentage increases in compressive strength at peak load

Specimens	Compressive strength	% increase	Compressive strength	% increase
Control		-		-
SF of 0.4 %		15		16
SF of 0.75%	20 MPa	26	30 MPa	28
SP of 0.8 %		11		13
SP of 1.8 %		25		30

4.2. Finite Element (FE) Modeling

In this study, the concrete damage plasticity (CDP) model available in ABAQUS [19] is used to simulate the behavior of normal, fiber-reinforced concrete, and self-compacting concrete. CDP is a general model that can be updated to model plain and reinforced concrete subjected to monotonic, cyclic, or dynamic loading. The behavior of CDP consists from two parts: tensile and compressive [20].

Compressive behavior of concrete is described by the yield stress, defined in ABAQUS as a function of plastic strain and explained using tabular data. The initial point of plastic strain must be zero. The data from experimental tests are used in defining the nonlinear behavior of concrete. In ABAQUS, five parameters are used to define the yield surface.

- Dilation angle ψ : used to determine the plastic flow. A value of 30° was used.
- Eccentricity ε : is the rate at which the plastic potential function approaches the asymptote. The default value of 0.1 was used.
- f_{b0}/f_{c0} : the ratio of the initial biaxial compressive stress and the initial uniaxial compressive stress. The default value of 1.16 was used.
- K_c : the multiaxial behavior of the material model. The default value of $2/3$ was used.
- The viscosity parameter μ : used to get a good convergence. A value of $\mu = 10^{-7}$ was used [21].

A 10-nodes three-dimensional quadratic tetrahedral element (C3D10) is used to model the three types of concrete. It is a general-purpose element that has four integration points as shown in Figure 5.

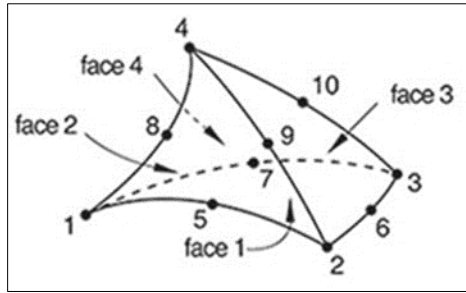


Figure 5. C3D10

The simulation consists of a concrete cylinder. The displacement and boundary conditions are applied as follows: nodes are constrained from movement on surface 1 in all directions, on surface 2 in the x and z-directions, while displacement in compression is applied at surface 3 as shown in Figure 6. Figure 7 describes the meshing of the model and Table 9 shows the FE governing parameters.

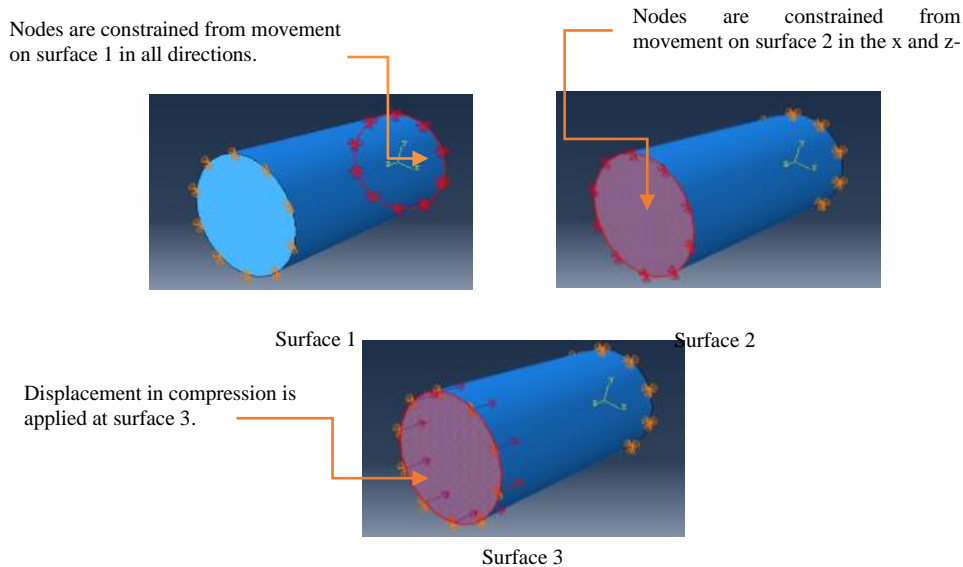


Figure 6. Boundary conditions for the tested concrete cylinders

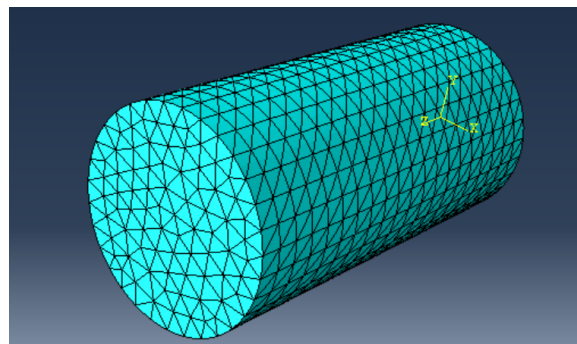


Figure 7. Meshing of the specimens

Table 9. FE governing parameters

FE governing parameters	Compressive Strength of 20 MPa					Compressive Strength of 30 MPa				
	Plain concrete	SFRC 0.4%	SFRC 0.75%	SCC 0.8%	SCC 1.8%	Plain concrete	SFRC 0.4%	SFRC 0.75%	SCC 0.8%	SCC 1.8%
Modulus of elasticity (MPa)	16334	23594	42469	15168	21779	19304	19737	33245	18875	35391
Stress-strain relationship	From Test	From Test	From Test	From Test	From Test	From Test	From Test	From Test	From Test	From Test
Poisson's ratio	0.2	0.2	0.2	0.2	0.2	0.2	0.2	0.2	0.2	0.2

4.3. Finite Element Results and Discussions

Figures 8 and 9 show stress-strain behavior from experimental and FE analyses for concrete with 20 MPa and 30 MPa of compressive strength, respectively, with steel fiber of 0, 0.4, and 0.75%, and SIKAVISCOCRETE-5930 IQ of 0, 0.8, and 1.8% by weight of concrete. The FE model exhibits a good prediction of the compressive behavior of plain concrete, steel fibers (SFRC), and concrete containing SIKAVISCOCRETE-5930 IQ. Table 10 lists the results coming out of the experimental and FE analysis at peak for concrete with compressive strengths of 20 MPa and 30 MPa. The percentage of difference in strength is calculated according to Equation 1.

$$\text{The percentage of difference} = \{(Test-FE) / \text{mean}\} * 100 \tag{1}$$

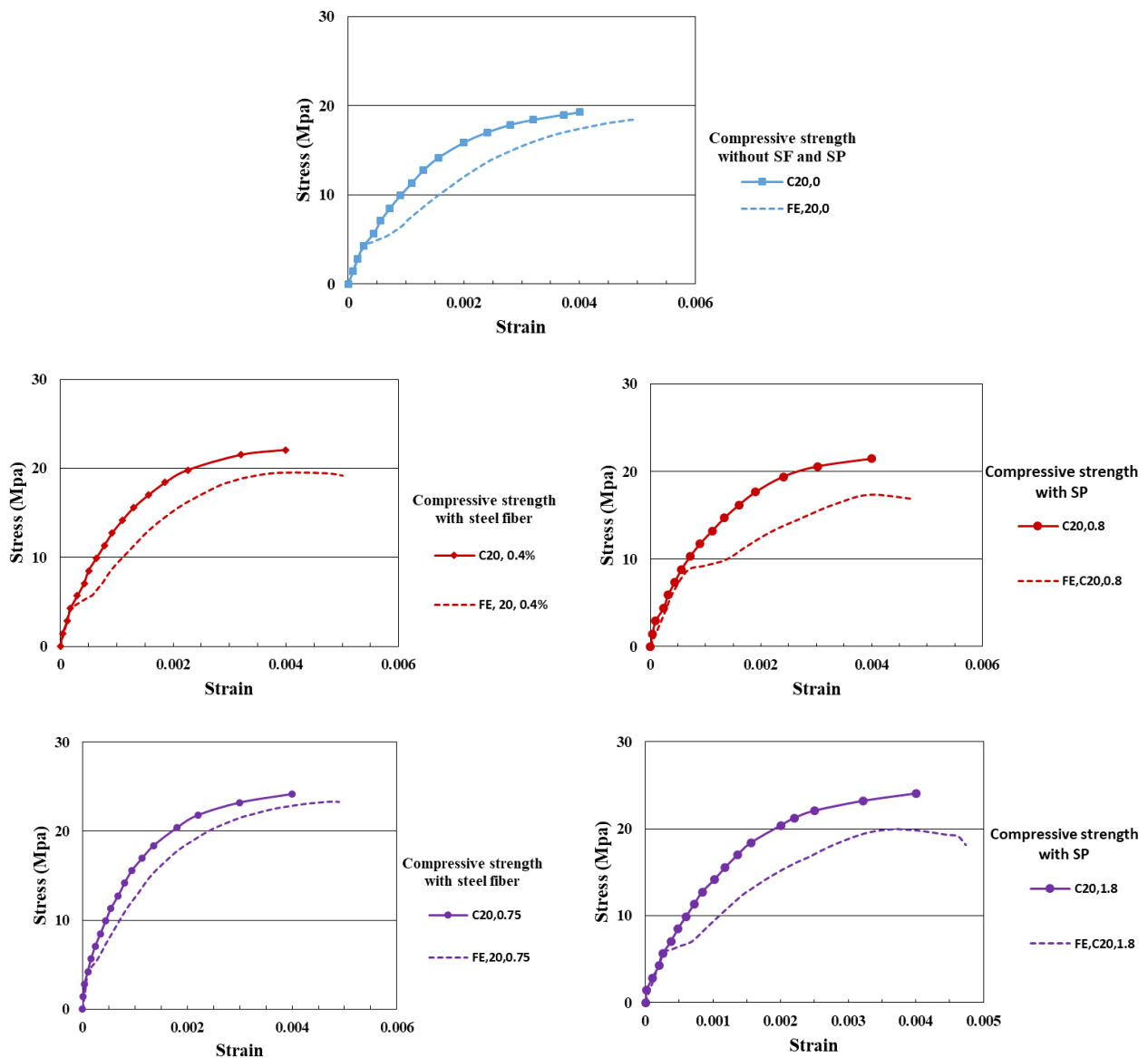


Figure 8. Stress-Strain curve for concrete with compressive strength of 20 MPa

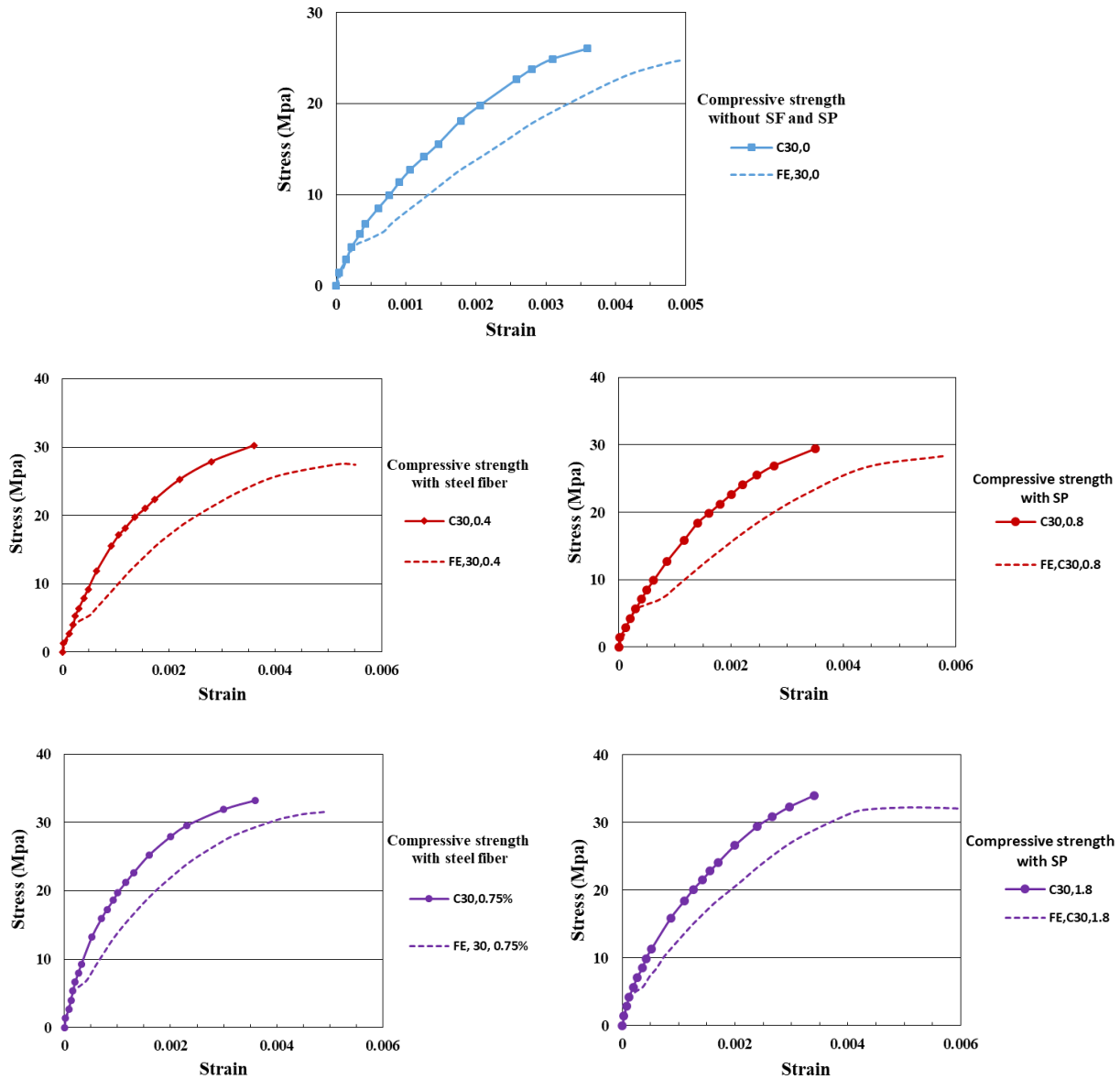


Figure 9. Stress-Strain curve for concrete with compressive strength of 30 MPa

Table 10. Strength from test and FE analysis

Concrete Compressive Strength	20 MPa				30 MPa				
	Specimens	Test	FE	T/FE	% differences (Eq. 1)	Test	FE	T/FE	% differences (Eq. 1)
20 MPa	Control	19.25	18.4	1.05	4.5	26.04	24.7	1.05	5.3
	SF of 0.4 %	22.08	19.54	1.13	12.2	30.26	27.4	1.10	9.9
	SF of 0.75%	24.1	23.3	1.03	3.4	33.24	31.5	1.06	5.4
30 MPa	Control	19.25	18.4	1.05	4.5	26.04	24.7	1.05	5.3
	SP of 0.8 %	21.4	17.3	1.24	21.1	29.44	28.39	1.04	3.6
	SP of 1.8 %	24.06	19.97	1.20	18.5	33.9	32.7	1.04	3.6

Figures 10-a and 10-b compare the ultimate loads from experimentally tested specimens with those obtained from FE analyses for concrete compressive strengths of 20 and 30 MPa with steel fibers of 0, 0.4, and 0.75% and SIKAVISCOCRETE-5930 IQ of 0, 0.8, and 1.8%.

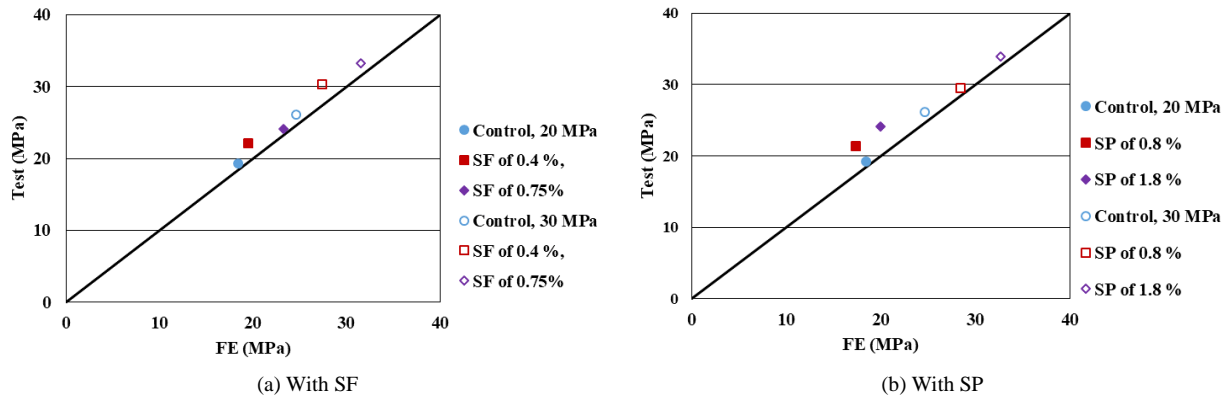


Figure 10. Test versus FE for the tested specimens

The statistical parameters (maximum, minimum, mean, standard deviation (STD), and coefficient of variation (COV)) are given in Table 11. A student’s t-test was conducted, and the results indicate that the difference between experimental and numerical results is not statistically significant, meaning that there is an acceptable agreement between them (Table 12).

Table 11. Applied statistical parameters

Specimens	Test MPa	FE MPa	T/FE	Test MPa	FE MPa	T/FE
Compressive strength	20 MPa (with SF)			30 MPa (with SF)		
Max	24.1	23.3	1.13	33.24	31.5	1.100
Min	19.25	18.4	1.03	26.04	24.7	1.05
Mean	22.08	19.54	1.046	30.26	27.4	1.100
STD	2.44	2.56	0.052	3.62	3.42	0.029
COV	0.11	0.13	0.050	0.12	0.12	0.027
Compressive strength	20 MPa (with SP)			30 MPa (with SP)		
Max	24.06	19.97	1.24	33.9	32.7	1.05
Min	19.25	17.2	1.05	26.04	24.7	1.04
Mean	21.4	18.4	1.205	29.44	28.39	1.037
STD	2.40	1.34	0.102	3.94	4.00	0.010
COV	0.112	0.07	0.085	0.13	0.14	0.010

Table 12. Student’s t-test

Concrete compressive strength	P-value	Comments
20 MPa with SF	0.2814	Statically insignificant
30 MPa with SF	0.3762	Statically insignificant
20 MPa with SP	0.1317	Statically insignificant
30 MPa with SP	0.7709	Statically insignificant

For all specimens made of plain, SFRC, and SCC with a strength of (20 and 30) MPa, the Student’s t-test exhibited statistically insignificant results, indicating that the FE model closely matches the experimental results. Test/calculated values (T/FE) exhibited a small variation through these groups ranging from 1.03 to 1.10 for SF specimens and from 1.04 to 1.24 for SP specimens, showing that the FE model predicted the strength accurately. Therefore, the FE model gives a reliable method for estimating the compressive strength of different concrete mixtures with no requirement for recalibration.

Finite element contours for concrete cylinders with a compressive strength of 20 MPa, a steel fiber of 0.4% and 0.75%, and SIKA-VISCOCRETE-5930 IQ of 0.8% and 1.8% are visualized as an axial stress (S33) as displayed in Figure 11. Generally, the stress intensity is higher at the edge where the load is applied and gradually decreases towards the center. The brittle nature of concrete leads the cracks to initiate at the surface until failure.

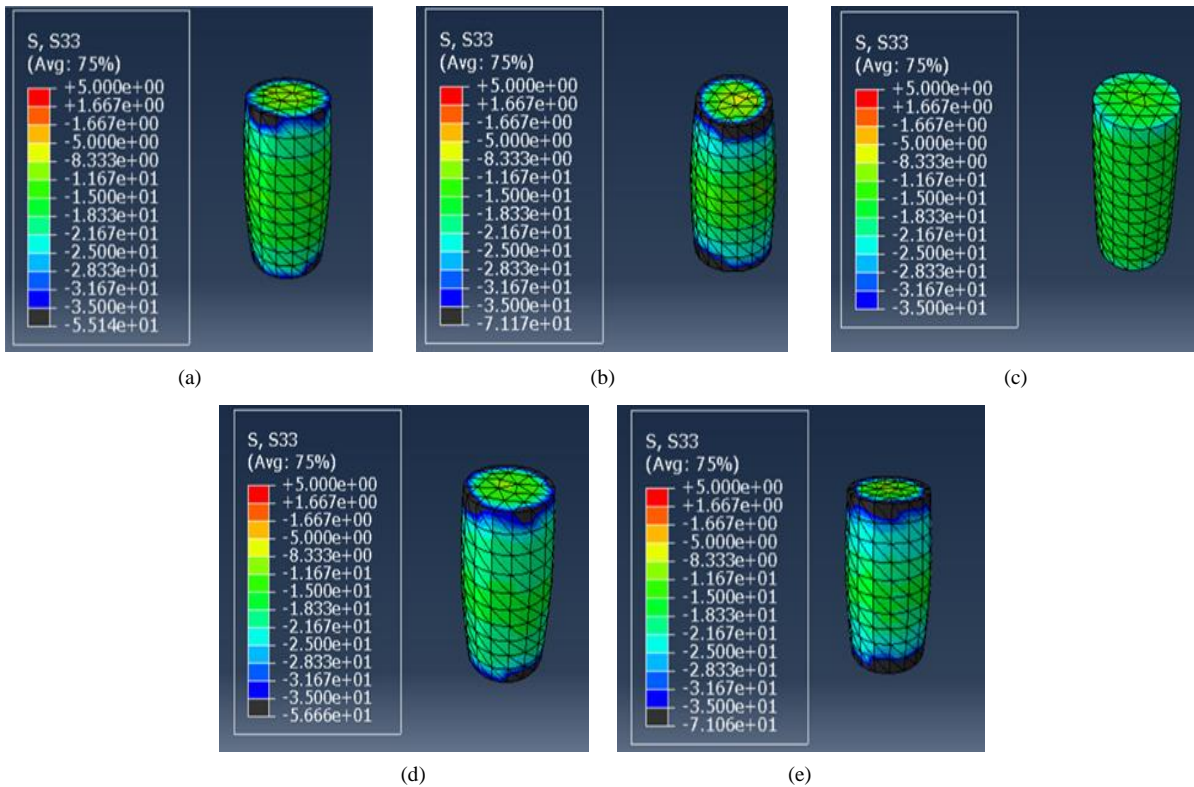


Figure 11. Finite element contours visualized the axial stress (S33) for: a. plain concrete, b. SFRC with 0.4% fiber, c. SFRC with 0.75% fiber, d. SCC with 0.8 % Sika-VISCOCRETE-5930 IQ , e. SCC with1.8 % Sika-VISCOCRETE-5930 IQ

4.4. Stress-Strain Relationship Under Different Confinement Levels

Two specimens were selected to study their behavior under various confinement levels. The first specimen of 20 MPa compressive strength and the steel fiber content is 0.4% while the second specimen of 30 MPa compressive strength and the superplasticizer content is 1.8%. Figure 12 shows the concrete block cylinder for the selected specimen under confinement.

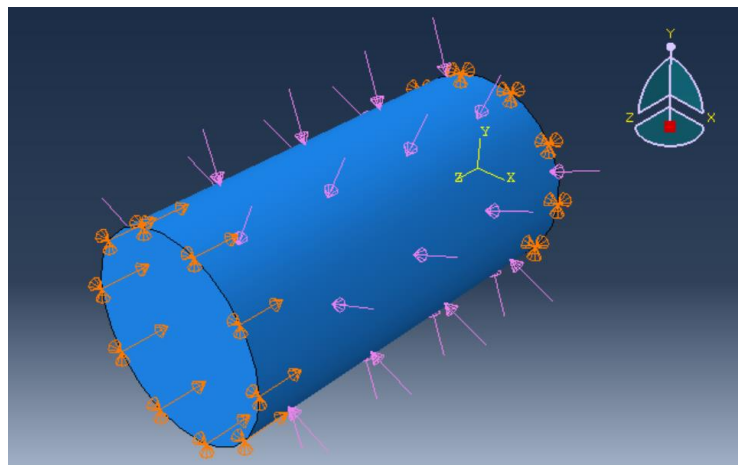


Figure 12. Concrete cylinder under confinement

For the first specimen, four hydrostatic stresses were applied to the concrete block cylinder. Hydrostatic stresses of 0, 1, 2, and 5 MPa under compressive displacement were studied; the results are shown in Figure 13-a. It illustrates how increased confinement raises the maximum stress that can be reached in the axial and lateral axes. Figure 13-a further illustrates how raising confining stresses causes the lateral strains (strain in x and y directions, ϵ_{11} and ϵ_{22}) to decrease, which in turn influences volumetric strain (summation of strain in lateral and longitudinal directions, $\epsilon_{11} + \epsilon_{22} + \epsilon_{33}$), as seen in Figure 14-a. The behavior of volumetric strain changes from compression dilation to compression as confining stresses are increased [22]. Similar behavior was exhibited by the second specimen, as shown in Figures 13-b and 14-b.

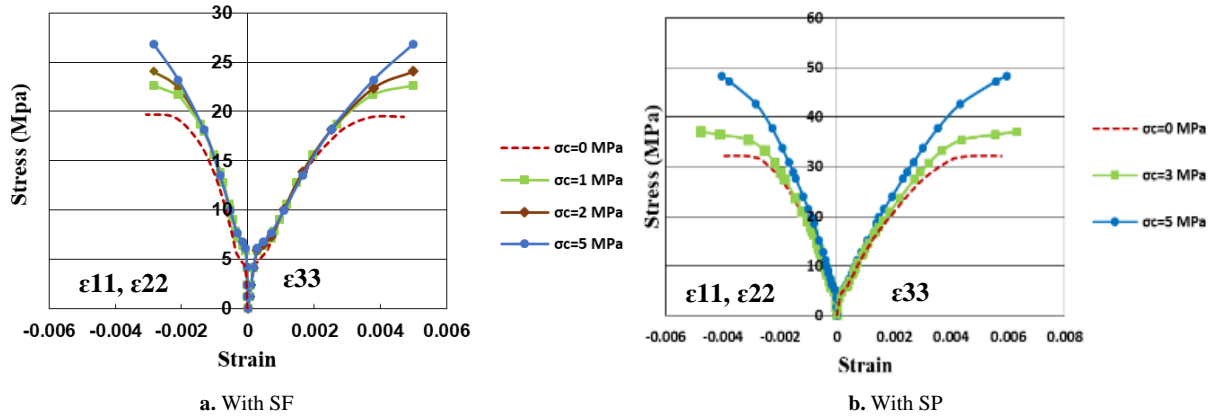


Figure 13. Stress versus strain under confinement in compression

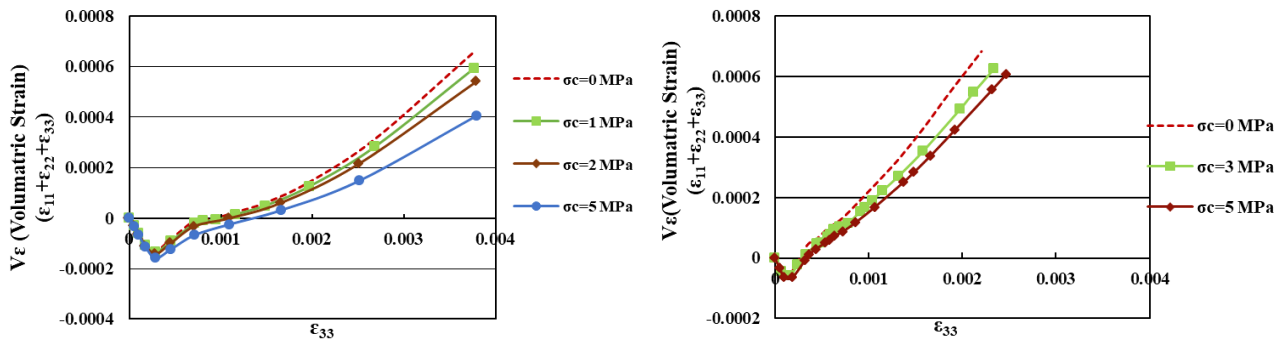
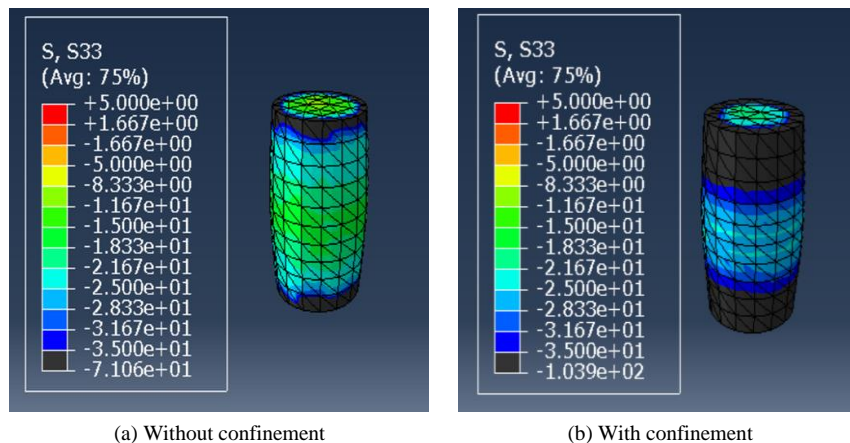


Figure 14. Volumetric strain versus axial strain

The above analysis is very significant for the FE model. The results from hydrostatic confinement analysis exhibit the accuracy of the FE model in predicting the increase in maximum stress and the change in strain behavior under confinement pressure. This shows that the FE model can accurately capture the effect of confinement pressure and represent how the material behaves under different situations.

Finite element contours for concrete cylinders with a compressive strength of 20 MPa and SIKA-VISCOCRETE-5930 IQ of 1.8% are visualized as stress (S33) in Figures 15-a and 15-b without and with confinement. For unconfined concrete, the axial stress (S33) gradient in steep shows a reduction from ends towards the center, while the stress distribution is more uniform for the confined cylinder. Confinement increases the axial stress at the center. Additionally, it limits the radial deformation, causing a redistribution of the axial stress and a decrease of the gradient between the surface and the center. When comparing the contour lines of the confined to the unconfined cylinder, the contour lines of the confined cylinder exhibit less variation with more uniform distribution from the center to the surface. Furthermore, the stress concentration is more at the ends and drops rapidly at the center. The uniform distribution of the axial stress improves both the capacity and stability of the concrete.



(a) Without confinement

(b) With confinement

Figure 15. Finite element contours stress (S33)

5. Conclusion

The data from the FE analysis are well corresponded with the experimental ones, and thus the model can be satisfactorily used to estimate the stress-strain characteristics of concrete in compression. Based on the Student's t-test, the difference between the experimental and FE results was insignificant, which also confirmed the accuracy of the model.

The influence of SFRC and SCC on stress-strain response was also notified in the research. Increased amounts of added steel fibers enhanced the ductility and crack resistance of concrete, resulting in smoother and gradual post-peak behavior. Similarly, the enhanced workability of SCC, which is attributed to the improved particle distribution, increased the compressive strength and the stress concentration.

In addition, the FE model accurately captured the behavior of concrete under various confinement levels, matching the earlier experimental findings. The influence of steel fibers and SCC develops the structural efficiency by improving the material's ability to resist cracking and deformation. Steel fibers helped manage crack growth, while SCC provided a denser and more uniform mixture, leading to an improved load distribution. With the increase in steel fibers and SCC, the stress-strain relationship showed enhanced performance in strength, ductility, and durability. These improvements validate that the approved FE model can act as an essential resource for optimizing mix designs, predicting structural performance, and minimizing the requirement for extensive experimental tests. Future studies may expand on this model to assess the anchorage effectiveness and failure modes of the tested specimens.

6. Declarations

6.1. Author Contributions

Conceptualization, M.M.A.H. and S.M.A.H.; methodology, H.S.A.; software, M.M.A.H.; validation, S.M.A.H. and H.S.A.; formal analysis, M.M.A.H.; investigation, S.M.A.H.; resources, H.S.A. and M.M.A.H.; data curation, H.S.A.; writing—original draft preparation, M.M.A.H. and S.M.A.H.; writing—review and editing, H.S.A.; visualization, M.M.A.H., S.M.A.H., and H.S.A.; project administration, M.M.A.H.; funding acquisition, M.M.A.H., S.M.A.H., and H.S.A. All authors have read and agreed to the published version of the manuscript.

6.2. Data Availability Statement

The data presented in this study are available in the article.

6.3. Funding

The authors received no financial support for the research, authorship, and/or publication of this article.

6.4. Conflicts of Interest

The authors declare no conflict of interest.

7. References

- [1] Yilmaz, S., & Ozmen, H. B. (2016). High Performance Concrete Technology and Applications. BoD—Books on Demand, Norderstedt, Germany. doi:10.5772/61562.
- [2] Vairagade, V. S., & Kene, K. S. (2013). Strength of normal concrete using metallic and synthetic fibers. *Procedia Engineering*, 51, 132–140. doi:10.1016/j.proeng.2013.01.020.
- [3] Choudhary, V. (2017). A Research Paper on the Performance of Synthetic Fibre Reinforced Concrete. *International Research Journal of Engineering and Technology*, 4(12), 1661–1663.
- [4] Mehta, P.K. and Monteiro, P.J.M. (2006) *Concrete: Microstructure, Properties, and Materials* (3rd Ed.) McGraw-Hill, New York, United States.
- [5] Abed, H. (2019). Production of Lightweight Concrete by Using Construction Lightweight Wastes. *Engineering and Technology Journal*, 37(1A), 12–19. doi:10.30684/etj.37.1a.3.
- [6] The Constructor. (2021). Fiber Reinforced Concrete - Types, properties and Advantages of Fiber Reinforced Concrete. The Constructor, Gopal Mishra. The Constructor, Zurich, Switzerland. Available online: <https://theconstructor.org/concrete/fiber-reinforced-concrete/150/> (accessed on February 2025).
- [7] Dawood, E. T., Abdullah, M. H., & Plank, J. (2022). The Influence of Hybrid Fibers and Nanomaterials (Nano Glass with Nano Slag) on the Behavior of Reactive Powder Concrete. *International Journal of Sustainable Construction Engineering and Technology*, 13(3), 159–173. doi:10.30880/ijscet.2022.13.03.015.
- [8] Dawood, E. T., & Al-Heally, M. S. F. (2021). Effect of recycled materials and hybrid fibers on the properties of self-compacting concrete. *Journal of Applied Engineering Science*, 19(1), 262–269. doi:10.5937/jaes0-28558.

- [9] Ayub, T., Khan, S. U., & Shafiq, N. (2018). Flexural Modelling and Finite Element Analysis of FRC Beams Reinforced with PVA and Basalt Fibres and Their Validation. *Advances in Civil Engineering*, 8060852. doi:10.1155/2018/8060852.
- [10] Rashidi, M., Kargar, S., & Roshani, S. (2024). Experimental and numerical investigation of steel fiber concrete fracture energy. *Structures*, 59, 105792. doi:10.1016/j.istruc.2023.105792.
- [11] Al_jubory, N., Ahmed, T., & Zidan, R. (2020). A Review on Mix Design of Self-Compacting Concrete. *Al-Rafidain Engineering Journal (AREJ)*, 25(2), 12–21. doi:10.33899/rengi.2020.126727.1017.
- [12] Akinpelu, M. A., Odeyemi, S. O., Olafusi, O. S., & Muhammed, F. Z. (2019). Evaluation of splitting tensile and compressive strength relationship of self-compacting concrete. *Journal of King Saud University - Engineering Sciences*, 31(1), 19–25. doi:10.1016/j.jksues.2017.01.002.
- [13] Chowdhury, Md. A., Islam, Md. M., & Ibna Zahid, Z. (2016). Finite Element Modeling of Compressive and Splitting Tensile Behavior of Plain Concrete and Steel Fiber Reinforced Concrete Cylinder Specimens. *Advances in Civil Engineering*, 6579434, 1–11. doi.:10.1155/2016/6579434.
- [14] Saffar, N. S. A., & Aghwan, A. A. A.-R. (2020). Nonlinear Finite Element Analysis of Shear Strength for Steel Fiber Reinforced Concrete I-Section Beams. *IOP Conference Series: Materials Science and Engineering*, 978, 012028. doi:10.1088/1757-899x/978/1/012028.
- [15] IQS. No. 5. (2019). Portland Cement. Iraqi Standard Specifications, Baghdad, Iraq.
- [16] IQS. No. 45. (1980). Natural Resources Aggregate Used in Concrete and Building. Iraqi Standard Specifications, Baghdad, Iraq.
- [17] ASTM C39/C39M-20. (2021). Standard Test Method for Compressive Strength of Cylindrical Concrete Specimens. ASTM International, Pennsylvania, United States. doi:10.1520/C0039_C0039M-20
- [18] ASTM C143/C143M-10. (2010). Standard Test Method for Slump of Hydraulic-Cement Concrete. ASTM International, Pennsylvania, United States. doi:10.1520/C0143_C0143M-10.
- [19] BS 1881-116. (1983) Testing Concrete. Method for Determination of Compressive Strength of Concrete Cubes. British Standard Institute (BSI), London, United Kingdom.
- [20] ABAQUS. (2009). Standard User's Manual. (Version 6.9). Dassault Systèmes, Vélizy-Villacoublay, France.
- [21] Malm, R. (2006). Shear cracks in concrete structures subjected to in-plane stresses. Ph.D. Thesis, KTH Royal Institute of Technology, Stockholm, Sweden.
- [22] Misra, A., & Pooorshojouy, P. (2015). Granular micromechanics model for damage and plasticity of cementitious materials based upon thermomechanics. *Mathematics and Mechanics of Solids*, 25(10), 1778–1803. doi:10.1177/1081286515576821.